Article:
Sarabadani Tafreshi, S, Ranjbar, M, Taghizade, N et al. (3 more authors) (2022) A First-Principles Study of CO2 Hydrogenation on a Niobium-Terminated NbC (111) Surface. ChemPhysChem, 23 (6). e202100781. ISSN 1439-4235

https://doi.org/10.1002/cphc.202100781

A first-principles study of CO_2 hydrogenation on Niobium-terminated NbC (111) surface

Saeedeh Sarabadani Tafreshi[1,*], Mahkameh Ranjbar[1], Narges Taghizade[2], S. F. K. S. Panahi[2], Maryam Jamaati[2], Nora H. de Leeuw[3,4]

[1]Department of Chemistry, Amirkabir University of Technology (Tehran Polytechnic), No. 350, Hafez Avenue, Valiasr Square, 1591634311 Tehran, Iran

[2]Department of Physics, Iran University of Science and Technology, Narmak, 16846-13114 Tehran, Iran

[3]School of Chemistry, Cardiff University, Main Building, Park Place, CF10 3AT Cardiff, UK

[4]School of Chemistry, University of Leeds, LT2 9JT Leeds, UK

[*]Corresponding author: s.s.tafreshi@aut.ac.ir

Abstract. As a promising material for the reduction of Greenhouse gas, Transition metal carbides which are highly active in the hydrogenation of CO_2 are mainly considered. In this regard, the reaction mechanism of CO_2 hydrogenation to useful products on the Nb-terminated NbC (111) surface is investigated by applying density functional theory calculations. The computational results display that formation of CH_4, CH_3OH and CO are more favored than other compounds, where CH_4 is the dominant product. In addition, the findings from reaction energies reveal that the preferred mechanism for CO_2 hydrogenation is thorough $HCOOH^*$ where the largest exothermic reaction energy releases during $HCOOH^*$ dissociation reaction (2.004eV). The preferred mechanism of CO_2 hydrogenation towards CH_4 production is $CO_2^* \rightarrow$ t,c-$COOH^* \rightarrow HCOOH^* \rightarrow HCO^* \rightarrow CH_2O^* \rightarrow CH_2OH^* \rightarrow CH_2^* \rightarrow CH_3^* \rightarrow CH_4^*$ where $CO_2^* \rightarrow$ t,c-$COOH^* \rightarrow HCOOH^* \rightarrow HCO^* \rightarrow CH_2O^* \rightarrow CH_2OH^* \rightarrow CH_3OH^*$ and $CO_2^* \rightarrow$ t,c-$COOH^* \rightarrow CO^*$ are also found as the favored mechanisms for CH_3OH and CO productions thermodynamically, respectively. During the mentioned mechanisms the hydrogenation of CH_2O^* to CH_2OH^* has the largest endothermic reaction energy of 1.344 eV.

It is also found from the electronic properties calculations that Nb-terminated NbC (111) is a suitable catalyst for CO_2 hydrogenation where adsorption and activation of CO_2 and also desorption of final products can be easily done on the surface, which is of crucial importance.

Keywords: CO_2 hydrogenation, DFT, NbC, Transition Metal Carbide

1. Introduction

In recent years, the amount of carbon dioxide (CO_2) in the atmosphere has increased due to the industrial revolution, in addition, to the use of fossil fuels as one of the major sources of energy in human life[1]. Carbon dioxide plays an important role in air pollution, global warming, and climate change, which causes many environmental problems such as moisturizing the air, damaging plants, etc.[2]. Therefore, the adsorption, activation, storage, and conversion of CO_2 into valuable products for environmental reasons has attracted the attention of many researchers[3]. Extensive researches have dealt with the conversion of CO_2 into alternative suitable hydrocarbon fuels such as methanol (CH_3OH), methane (CH_4), formic acid (HCOOH), and formaldehyde (CH_2O) [4, 5].

Since the CO_2 molecule has high chemical stability, relatively high adsorption energy is required to be completely adsorbed on the surface of a catalyst[6]. Moreover, the CO_2 molecule must be placed in a curved structure on the surface of the catalyst in which the charge can be transferred from the catalyst to the molecule for activation. Among the many catalysts that were studied theoretically, metal nanoparticles such as Ni, Pd, or Pt are commonly used in industry for CO_2 conversion. But, due to the complexity and high cost of these metals, researchers are looking for a new class of catalysts[7]. Besides, Pt catalysts are influenced by important problems such as oxidation, migration, loss of active surface area, corrosion of the carbon support, and reduction of activity due to impurities[8]. Alternatively, transition metal carbides (TMCs) with similar catalytic properties to Pt group metals have been vastly explored specially after work done by Levy and Boudart on tungsten carbides[9]. The unique physical and chemical properties of Transition metal carbides (TMCs) resulting from the combination of characteristics of covalent solids, ionic crystals, and transition metals[10] render them as a good alternative to precious Pt metal[11-20]. It is worth mentioning that TMC compounds show covalent solids hardness, the high melting temperature of ionic solids, and high electrical and thermal conductivity of transition metals[17, 21]. Hence, because of the fascinating properties and the lower cost of TMCs, they have been widely considered in recent decades in heterogeneous catalytic processes as catalysts or protectors of metal catalysts[6]. Tailoring TMC catalytic properties, the subject of many types of research in the field of catalyst and surface science, indicate that they are highly active in hydrogenating CO_2 and converting it to CH_3OH, CH_4 and CO[15, 22, 23]. Also, studies on CO_2 adsorption on TMC surfaces have revealed that some TMCs absorb CO_2 well and cause C-O bond dissociation lonely or in the presence of hydrogen[3, 23]. One of the widely used compounds in the TMC family which possess high hardness, high melting point, toughness, stiffness, and excellent chemical stability with moderate

catalytic activity is Niobium carbide (NbC) [24, 25]. Likewise to the NaCl structure, contains interpenetrating metal and carbon fcc lattices with the different crystalline planes. Another essential point of applying NbC is related to being chemically inert in reaction mechanisms which is a crucial feature of catalyst materials. The (111) surface with alternate termination of either by metal or by carbon is one of the most commonly studied crystalline planes[9]. It can be attributed to the fact that available energy levels around the Fermi surface at fcc (111) are higher in TMCs, which make this plane more active[21].

Though several studies on adsorption and activation of CO_2 by TMCs such as ZrC, NbC, TaC, WC, and TiC already exist in the literature[20, 23, 26, 27], no comprehensive DFT study of CO_2 hydrogenation has ever been done on these surfaces. The aim of the present study is the investigation of the electronic structure of NbC with fcc (111) surface as a candidate for activation and adsorption of CO_2. Moreover, in this study, we examine the hydrogenation mechanism of CO_2 to formic acid (HCOOH), formaldehyde (H_2CO), carbon monoxide (CO), methanol (CH_3OH), and methane (CH_4).

2. Model and Method

In this section, we illustrate details needed for our investigation. We have performed density functional calculation as implemented in the Vienna Ab initio Simulation Package (VASP) [28, 29]. The total energy calculations have been performed using the Perdew-Burke-Ernzerhof (PBE)[30, 31] form of the generalized gradient approximation (GGA) with the projector augmented wave (PAW) method[32, 33]. As shown in the literature[34], the inclusion of the long-range Van der Waals (vdW) force improves the energy description of each system. Therefore, we employed the DFT-D3[35] which is the method of Grimme as implemented in VASP. The electron wave functions are expanded using plane waves with a cutoff energy of 600 eV for bulk and slab structures, which high values ensured that no pulay stresses occurred within the cells during relaxation. The break condition for the ionic relaxation and electronic self-consistency loop as the convergence criteria for the residual force and energy of each atom during structure relaxations were set to 0.01 eV/Å and 10^{-5} eV, respectively. A vacuum space of more than 20Å is introduced to avoid interactions between periodic images. While 11×11×11 and 4×4×1 Monkhorst pack grids of k-points sample the Brillouin zone in the bulk and NbC (111) surface, respectively, the size of mesh grid in k space during electronic properties calculation is 20×20×2. The NbC (111) surface is modelled by a supercell containing 112 atoms and including seven layers which four bottom layers are fixed at the bulk position. A perpendicular dipole correction was applied to enhance energy convergence of the adsorbed systems.

In the end, the adsorption energy of adsorbates (E_{ads}) can be calculated as:

$E_{ads} = E_{A+slab} - E_A - E_{slab}$,

Where E_{A+slab}, E_A, and E_{slab} denote the total energies of the relaxed adsorbates on the surface complex, the isolated adsorbates, and NbC (111) slab, respectively. It is worth pointing that, a negative energy value demonstrates exothermic adsorption.

3. Results and Discussion

3.1. CO_2 adsorption geometry

Here, the understudy Nb-terminated structure among two possible surfaces of NbC (111), C-terminated NbC (111), and Nb-terminated NbC (111), is illustrated in Figure 1. a, where the slab used in our calculations is shown. The lowest-energy adsorption geometry for CO_2 molecule on the NbC (111) surface is presented in Figure 1. b, where the oxygen atoms of the CO_2 molecule tend to make a bond to Nb atoms of the surface with a bond length equal to 2.264 Å. It is noteworthy that placing CO_2 molecule over the NbC (111) significantly alters the structure of the molecule, where it can be clearly seen from Figure 1. c and d that the O–C–O bond angle decreases from 180° to 132° after adsorption of the molecule on the surface, resulting in the release of 1.863 eV energy. Adsorption of the CO_2 molecule also increases the bond length of C–O by approximately 8%.

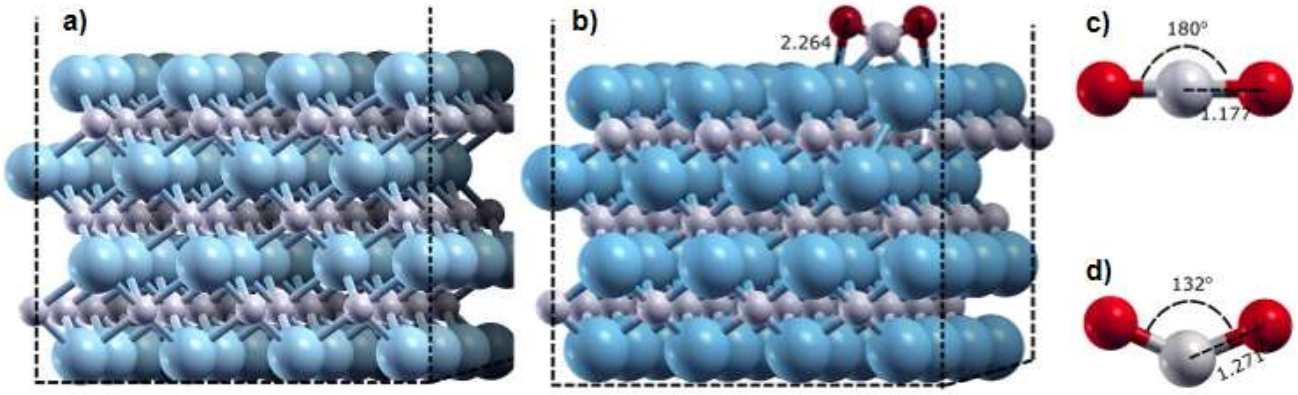

Figure 1. a) The NbC (111) surface, b) CO_2 adsorption geometry, c) the isolated CO_2 molecule and d) CO_2 geometry after adsorption.

3.2. CO_2 adsorption electronic properties

In order to accurately understand the CO_2 adsorption characteristic on the NbC (111) surface, the total density of state (TDOS) and charge densities are investigated. As shown in Figure 2. a, there are many states on the Fermi level and no energy gap is observed, which implies that NbC (111) surface

behaves like a metal. Since the behavior of the TDOS is quite similar to the behavior of Nb atoms, DOS, one can conclude that Nb atoms have a dominant contribution in the TDOS both above and below the Fermi level. Figure 2. b displays the changes occur after adding the CO_2 molecule on top of the surface, where the adsorption of the CO_2 molecule contributes mostly to the conduction band by increasing the TDOS.

To get a better insight on how charge distributes after adsorption of CO_2, the charge density differences[36] between the CO_2 + NbC (111) complexes and that of isolated slab and molecule is evaluated as follows:

$$\rho = \rho_{Molecule+NbC(111)} - \rho_{NbC(111)} - \rho_{Molecule},$$

Where $\rho_{Molecule+NbC(111)}$, $\rho_{NbC(111)}$, and $\rho_{Molecule}$ are the total charge of the relaxed adsorbates on the NbC (111) slab, the NbC (111) slab, and the isolated molecule, respectively. It is worth mentioning that the atomic positions kept the same as those of the total adsorbed one. The charge density difference plot in Figure 2. c demonstrates redistribution of charges in the system due to the adsorption. The positive charge difference is represented by green and the negative one by orange color. The sketched charge plot reveals the accumulation of negative charge around CO_2. Furthermore, the Bader charge analyses[37] after adsorption is shown for each atom of the CO_2 molecule (Figure 2. c). On one hand, the positive excess charge of +0.532 e^- is located on the C atom after adsorption, which was equal to +1.311e $^-$before adsorption occurrence. On the other hand, after the adsorption process, the negative charges of -0.655 e^- on the O atoms varies to -0.922 e^- and -0.914 e^-. Therefore, the negative excess charges on O atoms are increased after adsorption, while the positive charge of the Catom decreases due to adsorption, resulting in the accumulation of the net charge equal to -1.304 e^- around CO_2. Additionally, the charge redistribution of CO_2 adsorption over NbC (111), is calculated by means of the planar average charge density[38] difference $\Delta\rho(z)$, which is given as:

$$\Delta\rho(z) = \Delta\rho(z)_{Molecule+NbC(111)} - \Delta\rho(z)_{NbC(111)} - \Delta\rho(z)_{Molecule},$$

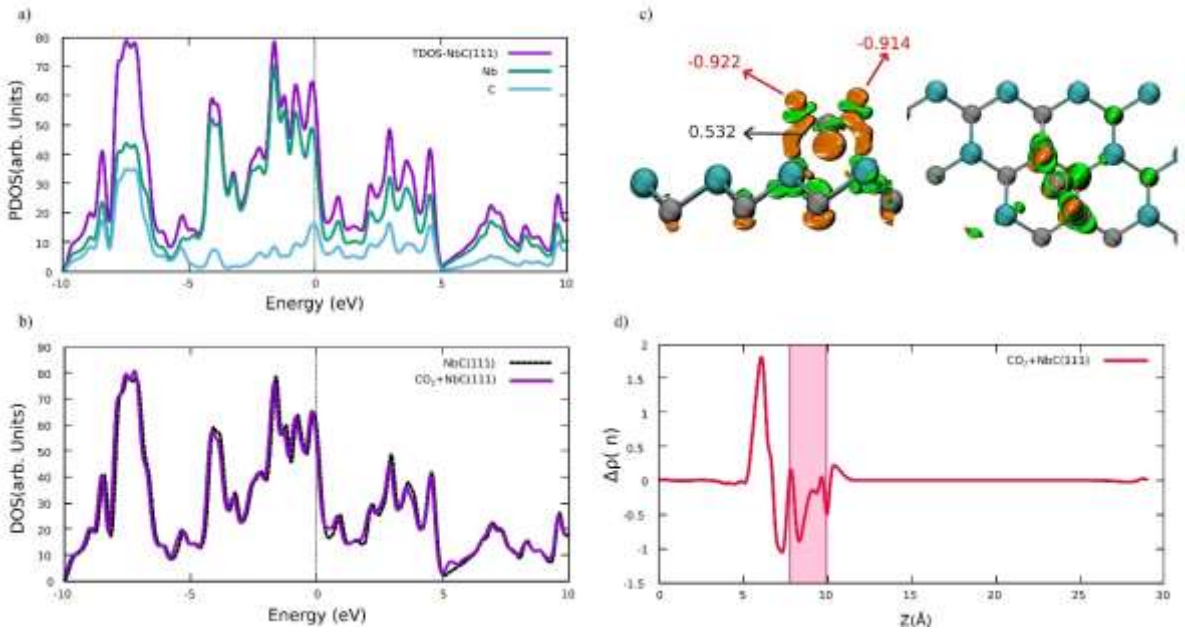

Figure 2. a) The partial density of state for NbC (111) surface, b) The total density of states of NbC (111) before and after adsorption of CO_2, c) The charge density differences of the CO_2 adsorbed structure in side and top view with the Bader charge of C and O atoms shown in grey and red (isovalue= ±0.01) and, d) The planar average charge density.

where $\Delta\rho(z)_{Molecule+NbC(111)}$, $\Delta\rho(z)_{NbC(111)}$, and $\Delta\rho(z)_{Molecule}$ are the planar average charge densities of the relaxed Molecule plus NbC(111) surface, NbC(111) slab and, the isolated CO_2 molecule, respectively. In Figure 2. d, highlighted region indicates the positions of CO_2 over NbC (111). Here negative (positive) values of $\Delta\rho(z)$ areas show the regions of charge accumulation (depletion), confirming that CO_2 gains charge after adsorption.

3.3. Chemical reactions

For further clarification, a detailed investigation of the reaction networks and their corresponding stable adsorption structures of all possible intermediates involved in the processes of CO_2 hydrogenation on NbC (111) surfaces is presented. Once CO_2 is placed on the surface, the hydrogenation process takes place in successive elementary chemical reactions, in which each species gains H^* to further produce the hydrogenated intermediate ones. The formic acid (HCOOH), formaldehyde (CH_2O), carbon monoxide (CO), methanol (CH_3OH), and methane (CH_4) are

produced[39, 40].

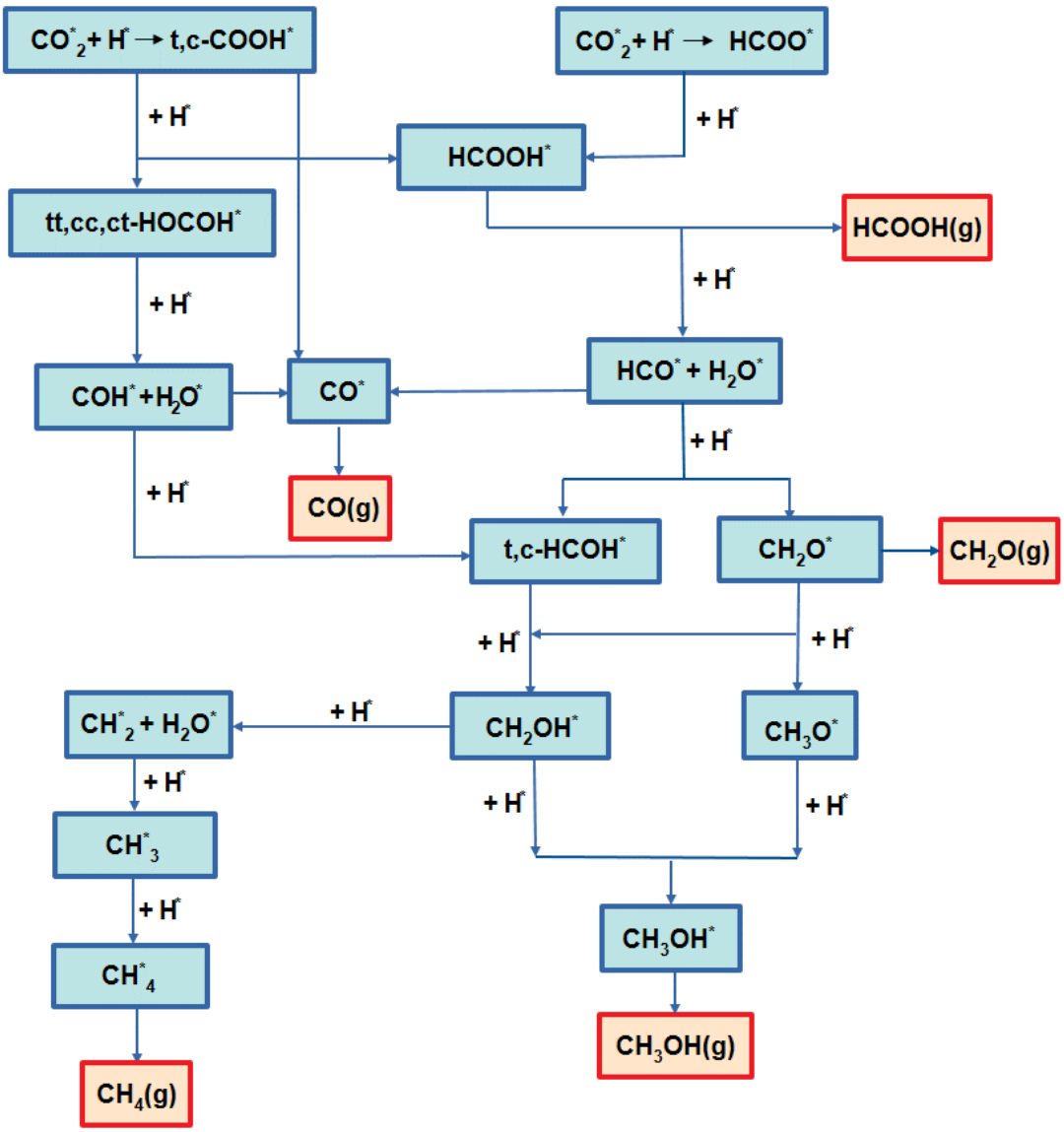

Figure 3. Possible reaction pathways for CO_2 hydrogenation to form HCOOH, CH_2O, CO, CH_3OH and CH_4 products.

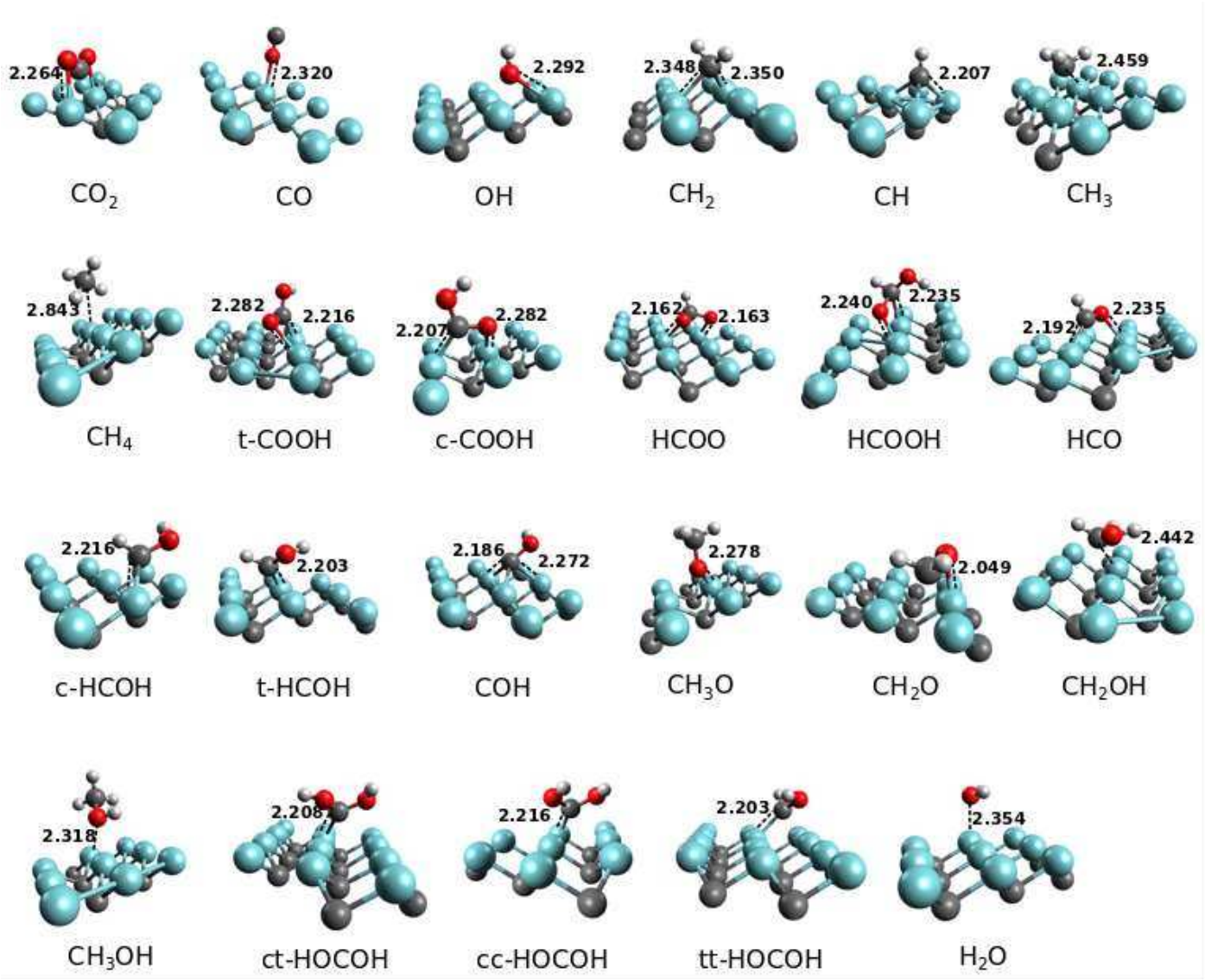

Figure 4. All possible adsorption geometries of reaction intermediates on the NbC (111), the distances are in Å.

These overall reactions are expressed as follows:

$CO_2 + 2H \rightarrow HCOOH$

$CO_2 + 4H \rightarrow CH_2O + H_2O$

$CO_2 + 6H \rightarrow CH_3OH + H_2O$

$CO_2 + 8H \rightarrow CH_4 + 2H_2O$

In this regard, Figure 3 describes the different paths where isolated CO_2 converges into HCOOH, CH_2O, CO, CH_3OH, and CH_4 compounds[1]. Based on the above-mentioned reaction formulas, we optimized all the adsorption configurations of intermediate structures on the NbC (111) surface. For

each adsorbate, the preferred adsorption site and the most stable geometry have been determined by putting the molecule on the surface in different positions. The preferred adsorption configuration with the most stable geometry and their relative energies are shown in table 1 and Figure. 4. Quesne et al.[41] showed that the chemically adsorption process occurs in the case of Nb-terminated NbC (111) surfaces, which is in agreement with our work. In other words, the Nb-terminated NbC (111) surface helps catalyze the chemical adsorption mechanism without any stable physically adsorbed states on NbC (111). Some earlier investigations also claimed that metal-terminated NbC surfaces are highly stable and can be considered as a privileged class of solid surfaces with the ability towards CO_2 reduction without any activation energy[41, 42]. In addition, the maximum overlap between dangling orbitals of atoms in the surface and atoms of the adsorbate happens due to the existence of central carbon atoms which fill the hollow sites between Nb atoms of NbC (111) surface.

The initial step of CO_2 hydrogenation is either the formation of the formate ($HCOO^*$) or the carboxyl species (trans-$COOH^*$ and/or cis-$COOH^*$). The formate prefers to bind at Nb site via an O–Nb bond with binding energy equal to -5.222 eV and an optimized bond length of 2.162 Å and 2.163 Å. Also, the calculated reaction energy of hydrogenation of CO_2 to HCOO is 0.062 eV, see Table 2 where we can find all the reaction energies of elementary hydrogenation steps. Once formate (HCOO) is formed, it can further hydrogenate to formic acid (HCOOH) via the reaction formula of $HCOO^* + H^* \rightarrow HCOOH^*$. This process has endothermic energy of 1.546 eV. $HCOOH^*$ is observed to be adsorbed stably on the NbC (111) with energy of -1.642 eV, in which O(C) atoms of $HCOOH^*$ bond with Nb atoms of the surface with 2.240 (2.235) Å.

On the other hand, CO_2 can also react with H to generate COOH with two cis and trans conformers via the formation of an O-H bond. These reactions are characterized as an endothermic process with energies of 0.899 eV and 0.925 eV for the cis and trans conformers, respectively. In the case of c-COOH, C tends to move toward the top of the C atom in NbC (111) resulting in two C–Nb and O–Nb bonds with bond lengths of 2.207 Å and 2.282 Å, respectively. While, the C atom in t-COOH is located approximately on top of the Nb atom of the surface leading to C–Nb with a bond length of 2.216 Å and O–Nb bond with a length of 2.282 Å. Moreover, both cis and trans conformers adsorbs perfectly on the Nb site via binding energies of -4.105 and -3.959 eV, respectively. Trans-COOH and cis-COOH could dissociate to CO^* and OH^* via the following reactions: $c\text{-}COOH^* \rightarrow CO^* + OH^*$, $t\text{-}COOH^* \rightarrow CO^* + OH^*$, which both of them are endothermic processes with reaction energies of 0.363 and 0.337 eV, respectively. CO prefers to adsorb at the top site of Nb atoms of the surface through its O atom, with the O–Nb bond length of 2.320 Å, and the adsorption energy of 0.351 eV. The C–O bond length elongates from 1.143Å in free CO to 1.159Å.

Subsequent hydrogenation products of carboxyl species (c-COOH and t-COOH) are dihydroxycarbene conformers (cc-HOCOH*, ct-HOCOH*, and tt-HOCOH*) where they adsorb stably on Nb site via carbon atoms with bond lengths (C-Nb) of 2.216, 2.208, and 2.203 Å with binding energies of -3.020, -2.876 and, -3.005 eV for cc-HOCOH*, ct-HOCOH*, and tt- HOCOH*, respectively. The elementary reactions of these steps are c,t-COOH* + H*→(ct, cc, tt)-HOCOH* which are endothermic reactions. The obtained reaction energies show that tt-HOCOH* conformer probably can be formed. On the contrary, the transformation of ct-HOCOH and cc-HOCOH to tt-HOCOH via reactions of ct-HOCOH*→tt-HOCOH* and cc-HOCOH*→tt-HOCOH* are exothermic with reaction energies of -0.124 and -0.215 eV, respectively.

Hydrogenation of carboxyl products may also lead to formic acid (HCOOH*) with reaction formula of c,t- COOH* + H*→HCOOH*. In this case, formic acid moves toward the Nb atom of the NbC surface. Both carbon and oxygen atoms are bonded to the Nb atom by making bonds of C–Nb and O–Nb with lengths of 2.235 and 2.240 Å, respectively. Comparing the lowest reaction energies among the aforementioned reactions, one can conclude that the HCOOH may be produced via the following reaction formula: t-COOH* + H*→ HCOOH*. As Figure. 3 shows, the formation of CH_3OH, and CH_4 can be achieved using possible pathways via HCOOH* or HOCOH*, which have been carefully studied and illustrated in the following.

Table 1. Adsorption energies of intermediates

Intermediate	Energy(eV)	Intermediate	Energy(eV)
CO_2	-1.863	CO	-0.353
OH	-5.427	CH_2	-5.797
CH	-7.404	CH_3	-3.721
CH_4	-0.298	t-COOH	-3.959
c-COOH	-4.105	HCOO	-5.222
HCOOH	-1.642	HCO	-4.240
c-HCOH	-2.797	t-HCOH	-4.042
COH	-4.977	CH_3O	-4.680
CH_2O	-2.797	CH_2OH	-3.293
CH_3OH	-0.959	ct-HOCOH	-2.876
cc-HOCOH	-3.020	tt-HOCOH	-3.005
H_2O	-0.997	...	...

3.3.1. Reaction Pathways of CO_2 to CH_3OH or CH_4 through $HCOOH^*$

As can be seen from Table 2, desorbing HCOOH ($HCOOH^* \rightarrow HCOOH$ (g)) is an endothermic process with required 1.642 eV energy, indicating that $HCOOH^*$ prefers not to desorb from the surface. In the next step, produced $HCOOH^*$ can be converted to HCO^* and OH^* through the decomposition reaction $HCOOH^* \rightarrow HCO^* + OH^*$ with an exothermic energy reaction of -1.25 eV. Therefore, the pathway after the formation of $HCOOH^*$ involves its separation into HCO^*, where the carbon and oxygen atoms of HCO^* approach the Nb atoms of the NbC surface with bond lengths of 2.191 Å and 2.235 Å, respectively, (see Figure. 4). HCO^* may dissociate to CO^* and H^* to further produce CO^*, this reaction is endothermic with a reaction energy of 1.659 eV.

Subsequent hydrogenation of HCO^* can lead to the formation of either formaldehyde (CH_2O^*) or $HCOH^*$ in cis and trans conformers. The former is produced throughout the $HCO^* + H^* \rightarrow CH_2O^*$ reaction formula with endothermic energy of 0.182 eV. The latter can be formed through two reactions of $HCO^* + H^* \rightarrow$ c-$HCOH^*$ and $HCO^* + H^* \rightarrow$ t-$HCOH^*$ with endothermic reaction energies of 1.137 and 1.213 eV, respectively. While, the oxygen atom of CH_2O^* is absorbed by the Nb atom leading to an O–Nb bond length of 2.049 Å, the carbon atoms of c-$HCOH^*$ and t-$HCOH^*$ species bond to the Nb atoms of the surface with C–Nb bond lengths of 2.216 Å and 2.203 Å, respectively. Since the conversion from c-$HCOH^*$ to t-$HCOH^*$ is an exothermic process with a reaction energy of -0.157 eV, the hydrogenation is more likely to be continued from t-$HCOH^*$.

Further hydrogenation of CH_2O^* leads to the formation of Hydroxymethyl (CH_2OH^*) or methoxy (CH_3O^*). This process occurs through $CH_2O^* + H^* \rightarrow CH_2OH^*$ and $CH_2O^* + H^* \rightarrow CH_3O^*$ formulas with the endothermic energies of 1.344 and 0.303 eV, respectively. As can be obviously seen from the Figure. 4, the carbon atom of CH_2OH^* at a distance of 2.442 Å binds to the NbC surface (C–Nb) while in the case of CH_3O^* the oxygen atom is adsorbed to the Nb atom with a bond length of 2.273 Å. Since hydrogenation from t-$HCOH^*$ to CH_2OH^* is energetically more favorable than that of CH_2O^*, CH_2OH^* forms via t-$HCOH^* + H^* \rightarrow CH_2OH^*$ rather than $CH_2O^* + H^* \rightarrow CH_2OH^*$ process.

CH_3O^* and CH_2OH^* can also be hydrogenated to methanol CH_3OH^* via $CH_3O^* + H^* \rightarrow CH_3OH^*$ and $CH_2OH^* + H^* \rightarrow CH_3OH^*$ where both reactions are endothermic with the energies of 1.739 and 0.698 eV, respectively. The methanol molecule is adsorbed on the NbC surface by its OH group, where the distance of its O atom and the nearest Nb atom is about 2.318 Å (Figure. 4). Therefore, the sequencing of elementary steps for methanol production from CO_2^* on the NbC surface via $HCOOH^*$ path will be as shown below:

$CO_2^* \rightarrow HCOO^*$, t,c-$COOH \rightarrow HCOOH^* \rightarrow HCO^* \rightarrow$ t,c-$HCOH^*$, $CH_2O^* \rightarrow CH_2OH^*$, $CH_3O^* \rightarrow CH_3OH^*$.

Dissociation of CH_2OH^* to CH_2^* ($CH_2OH^* \rightarrow CH_2^* + OH^*$) with exothermic reaction energy of -1.976 eV is another likely reaction, which leads to the methane (CH_4^*) production via subsequent hydrogenation of CH_2^* and CH_3^* through $CH_2^* + H^* \rightarrow CH_3^*$ and $CH_3^* + H^* \rightarrow CH_4^*$ reactions, respectively. The production of CH_3^* is an exothermic process with reaction energy of -0.009 eV, whereas the production of CH_4^* is an endothermic process of energy 1.137 eV. In CH_3^* and CH_4^* products, the carbon atoms prefer to bond with the Nb atoms of the surface, with the C–Nb bond lengths of 2.459 and 2.843 Å, respectively. Similar to the CH_3OH, the overall sequencing steps for CH_4^* production through HCOOH is indicated as follows:

$CO_2^* \rightarrow HCOO^*$, t,c-$COOH^* \rightarrow HCOOH^* \rightarrow HCO^* \rightarrow$ t,c-$HCOH^*$, $CH_2O^* \rightarrow CH_2OH^* \rightarrow CH_2^* \rightarrow CH_3^* \rightarrow CH_4^*$.

It is worth mentioning that during CH_3OH^* and CH_4^* production via HCOOH mechanism while the largest exothermic reaction energy of -2.004 eV occurs during the dissociation reaction of $HCOOH^*$ to HCO^*, the largest endothermic reaction energies belong to the hydrogenations of $HCOO^*$ to $HCOOH^*$ and CH_3O^* to CH_3OH^* with reaction energies of 1.546 and 1.739 eV respectively.

3.3.2. Reaction Pathways of CO_2 to CH_3OH or CH_4 through HOCOH.

As mentioned before, tt-$HOCOH^*$ is the preferred conformer of $HOCOH^*$ due to its lowest energy

compared to the two other ones (see Table 2). Dissociation of tt-HOCOH* results in the formation of COH*. In this exothermic process with reaction energy of -1.295 eV, tt-HOCOH* breaks into COH* and OH* through tt-HOCOH* → COH* + OH*. The carbon atom of COH* is connected to two Nb atoms of NbC surface with C–Nb bond lengths of 1.439 and 1.460 Å. Dissociation of COH* (COH* → CO* + H*) leads to the production of CO* and H*. This reaction is endothermic with a reaction energy of 0.468 eV. As discussed before, CO* could be also produced from the dissociation of HCO* and COOH* conformers. Among them, t-COOH* has the lowest endothermic energy, which means for the successive reactions steps for CO production on NbC surfaces, the feasible pathway is through dissociation of t-COOH*.

If COH* takes another hydrogen, it will convert to either trans-HCOH* or cis-HCOH* with endothermic energies of 0.023 and 0.179 eV, respectively. Then, CH_2OH^* and CH_3OH^* can be formed by further hydrogenation of t,c-HCOH*. Finally, the produced CH_2^*, resulting from the dissociation of CH_2OH^*, leads to the final products of CH_3^* and CH_4^*. Therefore, the following pathways contribute to the production of CH_3OH^* and CH_4^* via HOCOH*:

$CO_2^* \rightarrow$ t,c-COOH* → tt-HOCOH* → COH* → t,c-HCOH* → CH_2OH^* → CH_3OH^*.

$CO_2^* \rightarrow$ t,c-COOH* → tt-HOCOH* → COH* → t,c-HCOH* → CH_2OH^* → CH_2^* → CH_3^* → CH_4^*.

While the largest endothermic reaction energy is related to the hydrogenation of t,c-COOH* to different conformers of HOCOH*, the dissociation reactions of tt-HOCOH and CH_2OH^* have the largest exothermic reaction energies of -1.295 and -1.976 eV among other reactions in the production of CH_3OH^* and CH_4^* via HOCOH* mechanism.

For giving more details, the reaction energy values and profiles of different potential pathways are depicted in Figure 5. According to the mechanisms shown in Figure 5, the whole processes of all products formations are exothermic where CO*, CH_3OH^*, and CH_4^* are the dominant products which their reaction profiles are more favored thermodynamically. Since the released energy during the CH_4^* production is almost more than that of other products and dissociation of HCOOH* has the highest exothermic reaction with releasing the energy of 2.004 eV, formation of CH_4^* through HCOOH* intermediate is the most favored pathway.

Considering all the above, the preferred mechanism of CO_2 hydrogenation towards CH_4 production is $CO_2^* \rightarrow$ t,c-COOH* → HCOOH* → HCO* → CH_2O^* → CH_2OH^* → CH_2^* → CH_3^* → CH_4^*. The pathways of $CO_2^* \rightarrow$ t,c-COOH* → HCOOH* → HCO* → CH_2O^* → CH_2OH^* → CH_3OH^* and CO_2^* → t,c-COOH* → CO* are found as the favored mechanisms for CH_3OH and CO productions, respectively. Through all the preferred pathways, the hydrogenation of CH_2O^* to CH_2OH^* and HCOOH* dissociation have the highest endothermic and exothermic reaction energies of 1.344 and

2.004 eV, respectively.

Desorption of CH_3OH^*, $HCOOH^*$, CH_2O^*, CO^* and CH_4^* products need 0.959, 1.642, 2.797, 0.351, and 0.298 eV of energies, respectively, showing that CH_4^*, CO^* and CH_3OH^* species desorb from the surface easier than $HCOOH^*$ and CH_2O^*, helping to remove the products from the surface of the catalyst.

Table 2. Possible reactions and their corresponding energies in the hydrogenation of intermediates to form HCOOH, CH_2O, CO, CH_3OH and CH_4 Products.

Elementary Reactions	ΔE(eV)
$CO_2(g) \rightarrow CO_2^*$	-1.863
$CO_2^* + H^* \rightarrow HCOO^*$	0.062
$CO_2^* + H^* \rightarrow c\text{-}COOH^*$	0.899
$CO_2^* + H^* \rightarrow t\text{-}COOH^*$	0.925
$HCOO^* + H^* \rightarrow HCOOH^*$	1.546
$c\text{-}COOH^* \rightarrow CO^* + OH^*$	0.363
$t\text{-}COOH^* \rightarrow CO^* + OH^*$	0.337
$c\text{-}COOH^* + H^* \rightarrow HCOOH^*$	0.708
$t\text{-}COOH^* + H^* \rightarrow HCOOH^*$	0.682
$c\text{-}COOH^* + H^* \rightarrow cc\text{-}HOCOH^*$	1.406
$t\text{-}COOH^* + H^* \rightarrow tt\text{-}HOCOH^*$	1.165
$c\text{-}COOH^* + H^* \rightarrow ct\text{-}HOCOH^*$	1.314
$t\text{-}COOH^* + H^* \rightarrow ct\text{-}HOCOH^*$	1.288
$cc\text{-}HOCOH^* \rightarrow tt\text{-}HOCOH^*$	-0.215
$ct\text{-}HOCOH^* \rightarrow tt\text{-}HOCOH^*$	-0.124
$tt\text{-}HOCOH^* \rightarrow COH^* + OH^*$	-1.295
$COH^* \rightarrow CO^* + H^*$	0.468
$COH^* + H^* \rightarrow t\text{-}HCOH^*$	0.023
$COH^* + H^* \rightarrow c\text{-}HCOH^*$	0.179
$HCOOH^* \rightarrow HCO^* + OH^*$	-2.004
$HCO^* \rightarrow CO^* + H^*$	1.659
$HCO^* + H^* \rightarrow t\text{-}HCOH^*$	1.213
$HCO^* + H^* \rightarrow c\text{-}HCOH^*$	1.370
$HCO^* + H^* \rightarrow CH_2O^*$	0.182
$CH_2O^* + H^* \rightarrow CH_3O^*$	0.303
$CH_2O^* + H^* \rightarrow CH_2OH^*$	1.344
$t\text{-}HCOH^* + H^* \rightarrow CH_2OH^*$	0.312
$CH_3O^* + H^* \rightarrow CH_3OH^*$	1.739
$CH_2OH^* + H^* \rightarrow CH_3OH^*$	0.698
$CH_2OH^* \rightarrow CH_2^* + OH^*$	-1.976
$CH_2^* + H^* \rightarrow CH_3^*$	-0.009
$CH_3^* + H^* \rightarrow CH_4^*$	1.137
$CO^* \rightarrow CO(g)$	0.351
$HCOOH^* \rightarrow HCOOH(g)$	1.642
$CH_2O^* \rightarrow CH_2O(g)$	2.797
$CH_4^* \rightarrow CH_4(g)$	0.298
$CH_3OH^* \rightarrow CH_3OH(g)$	0.959
$H_2O^* \rightarrow H_2O(g)$	0.997

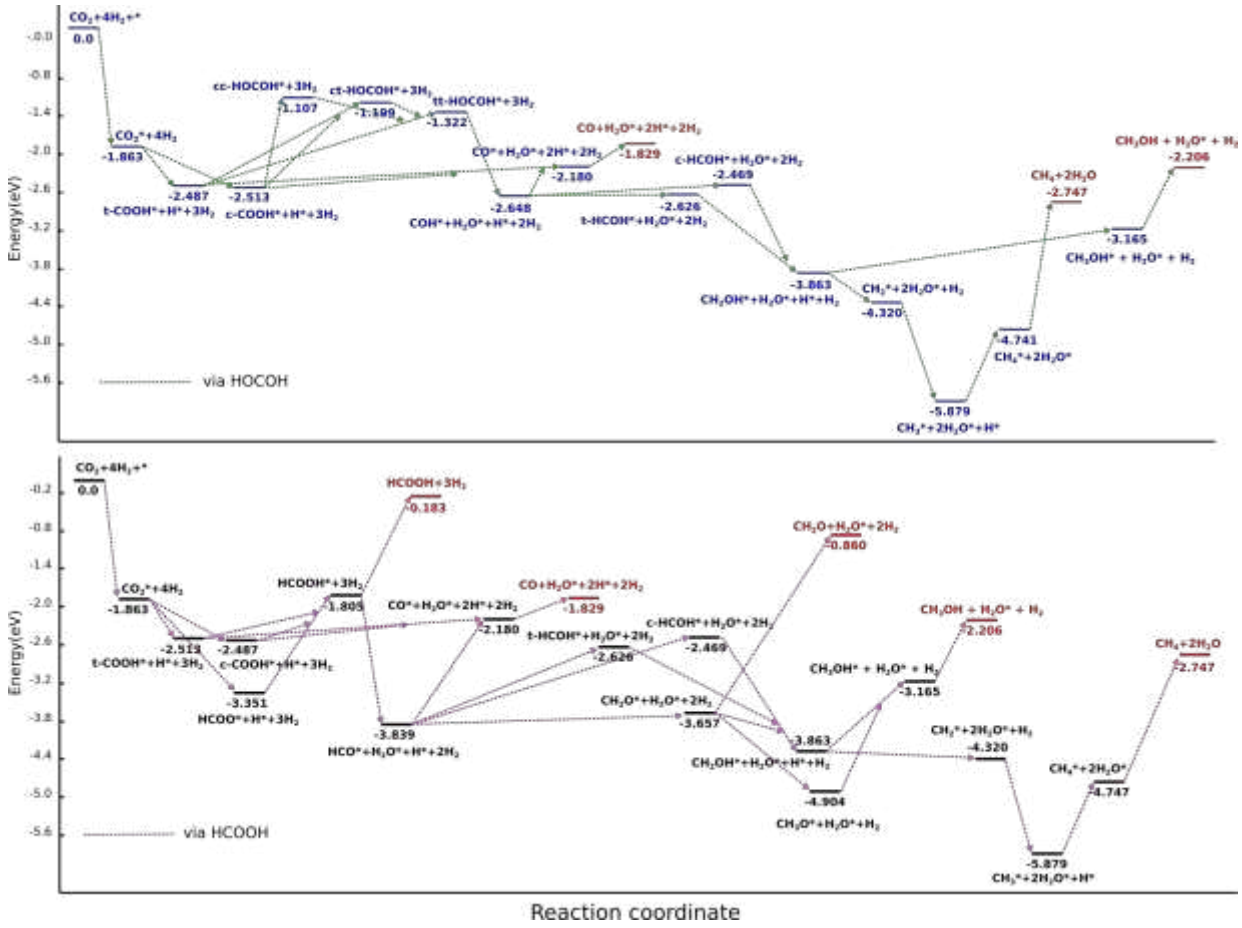

Figure 5. Reaction profile for CO_2 and subsequent hydrogenation of intermediates to CH_3OH and CH_4 via a) HOCOH and b) HCOOH on the NbC (111) surface. The indicated profiles are relative to the summation of the total free energy of the photocatalyst, CO_2, and four H_2 molecules in the gas phase [43].

3.4. Products electronic properties

To give a better insight into the desorption process, the TDOS and charge densities for the products of CH_4 and CH_3OH in Figures. 6 and 7 have been studied. As can be seen from Figure 6. a, total DOS is perfectly aligned in both the presence and absence of the CH_4 molecule, especially around the Fermi level. This fact indicates that the CH_4 molecule can be easily separated from the NbC (111) surface. Figure 7. a shows TDOS for another final product of the hydrogenation of the CO_2 molecule on NbC (111) surface. As can be seen, the CH_3OH molecule does not have much effect on NbC (111) TDOS, which means that this molecule can be easily extracted from the surface. Consequently, little changes in charge transfer also confirm that both CH_3OH and CH_4 molecules can easily desorb from the NbC (111) surface.

4. Conclusion

To conclude, we perform DFT calculations to study the CO_2 hydrogenation to HCOOH, CH_2O, CO, CH_3OH and, CH_4 products on NbC (111) surface. The calculated reaction energies revealed that Nb-terminated NbC (111) surface is a good candidate for catalyzing the CO_2 hydrogenation reactions. While CH_4 is the dominant product through the $HCOOH^*$ pathway as the favored mechanism, CH_3OH and CO productions are also favored. It is found that the largest exothermic reaction energy is related to the $HCOOH^*$ dissociation reaction, while the hydrogenation of CH_2O^* needs the highest endothermic reaction energy (1.344 eV). Larger desorption energies of $HCOOH^*$ and CH_2O^* species help to proceed the hydrogenation process on the surface and smaller those of CH_4^*, CH_3OH^* and CO^* result in desorption of these products from the surface easily. The electronic properties calculations confirmed that NbC (111) is a suitable catalyst for adsorption, activation, and hydrogenation of CO_2 and also for desorption of final materials. The kinetics calculations will also help us to get more insights into the hydrogenation mechanisms of CO_2.

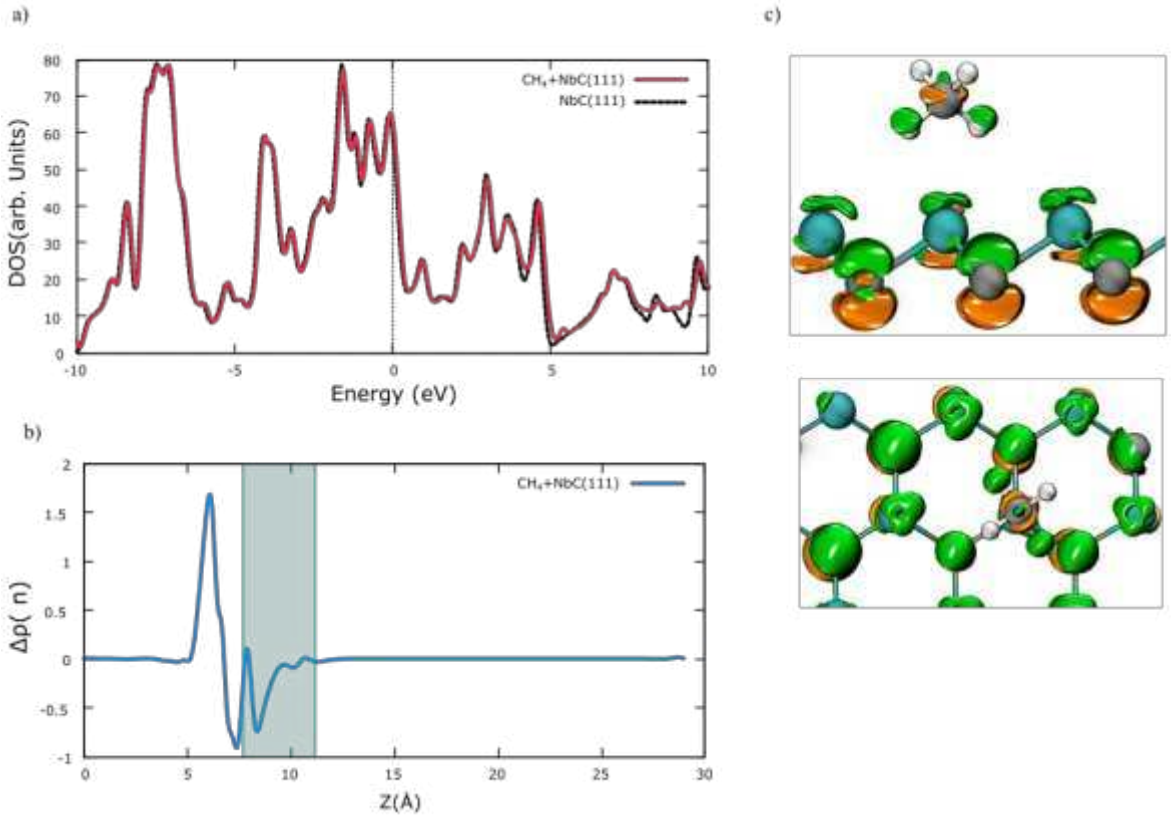

Figure 6. a) The total density of states, b) planer average charge density, and c) charge density difference for CH_4 product (isovalue = ±0.003).

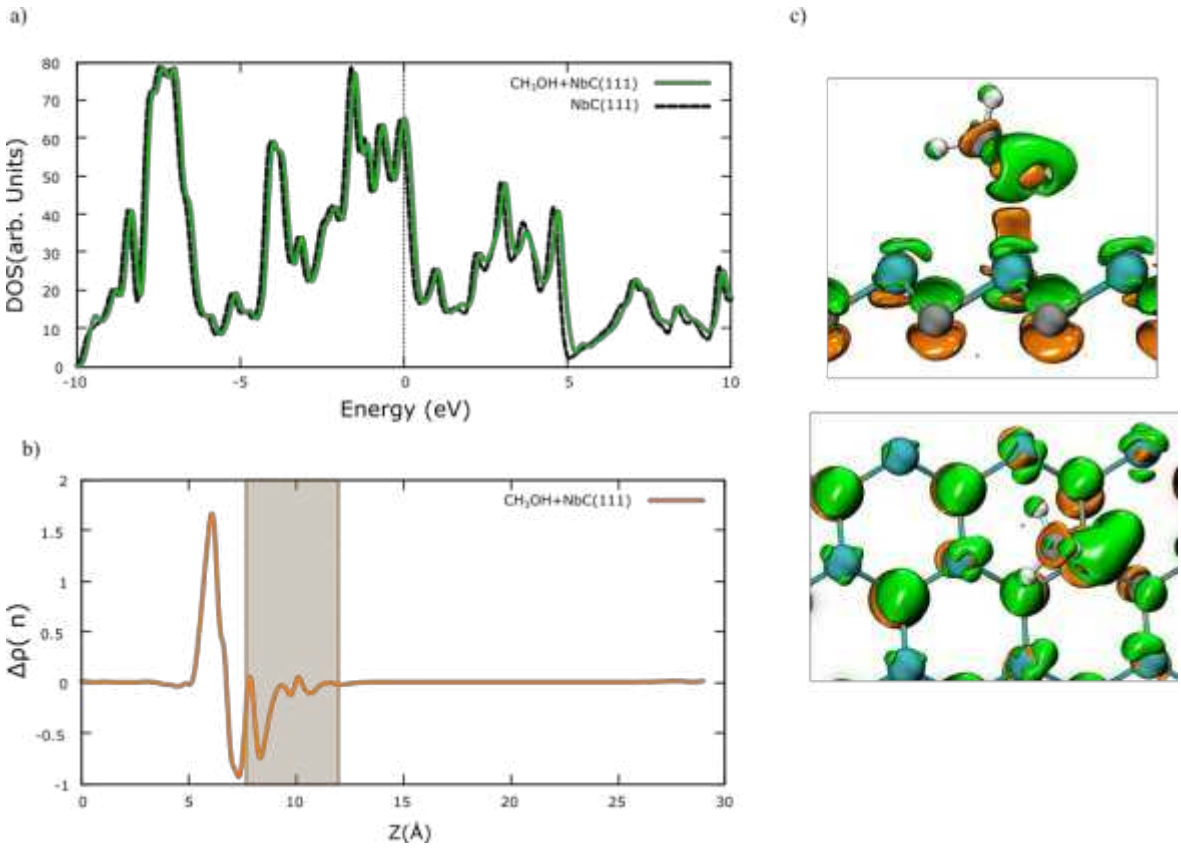

Figure 7. a) The total density of states, b) the planer average charge density, and c) charge density differences for CH_3OH product (isovalue = ±0.003).

Acknowledgments:

S.S.T thanks the Iran National Science Foundation (INSF) Grant No 97020912 for the financial support of this work. This work has used the computational facilities of the Advanced Research Computing at Cardiff (ARCCA) Division, Cardiff University, and HPC Wales.

5. References

[1] S. S. Tafreshi, A. Z. Moshfegh, N. H. de Leeuw, *J. Phys. Chem. C* **2019**, *123*, 22191-22201.
[2] R. Nataly Echevarria Huaman, T. Xiu Jun, *Renew. Sust. Energ. Rev.* **2014**, *31*, 368-385.
[3] S. Posada-Pérez, P. J. Ramírez, J. Evans, F. Viñes, P. Liu, F. Illas, J. A. Rodriguez, *J. Am. Chem. Soc.* **2016**, *138*, 8269-8278.
[4] Z. Jiang, W. Wan, H. Li, S. Yuan, H. Zhao, P. K. Wong, *Adv. Mater.* **2018**, *30*, 1706108.
[5] T. Ohno, N. Murakami, T. Koyanagi, Y. Yang, *J. CO2 Util.* **2014**, *6*, 17-25.
[6] X. Liu, C. Kunkel, P. Ramírez de la Piscina, N. Homs, F. Viñes, F. Illas, *ACS Catal.* **2017**, *7*, 4323-4335.
[7] J. A. Rodriguez, J. Evans, L. Feria, A. B. Vidal, P. Liu, K. Nakamura, F. Illas, *J. Catal.* **2013**, *307*, 162-169.
[8] C. Sealy, *Mater. Today* **2008**, *11*, 65-68.
[9] H. H. Hwu, J. G. Chen, *Chem. Rev.* **2005**, *105*, 185-212.
[10] F. Viñes, C. Sousa, P. Liu, J. A. Rodriguez, F. Illas, *J. Phys. Chem. C* **2005**, *122*, 174709.
[11] R. B. Levy, M. Boudart, *Science* **1973**, *181*, 547.
[12] J. B. Claridge, A. P. E. York, A. J. Brungs, C. Marquez-Alvarez, J. Sloan, S. C. Tsang, M. L. H. Green, *J. Catal.* **1998**, *180*, 85-100.
[13] S. V. Didziulis, P. Frantz, S. S. Perry, O. El-bjeirami, S. Imaduddin, P. B. Merrill, *J. Phys. Chem. B* **1999**, *103*, 11129-11140.
[14] Á. Koós, F. Solymosi, *Catal. Lett.* **2010**, *138*, 23-27.
[15] S. Posada-Pérez, F. Viñes, P. J. Ramirez, A. B. Vidal, J. A. Rodriguez, F. Illas, *PCCP* **2014**, *16*, 14912-14921.
[16] F. Viñes, J. A. Rodriguez, P. Liu, F. Illas, *J. Catal.* **2008**, *260*, 103-112.
[17] S. T. Oyama, *Catal. Today* **1992**, *15*, 179-200.
[18] R. Barthos, F. Solymosi, *J. Catal.* **2007**, *249*, 289-299.
[19] L. Li, D. S. Sholl, *ACS Catal.* **2015**, *5*, 5174-5185.
[20] S. Posada-Pérez, F. Viñes, J. A. Rodriguez, F. Illas, *Top. Catal.* **2015**, *58*, 159-173.
[21] L. I. Johansson, *Surf. Sci. Rep.* **1995**, *21*, 177-250.
[22] M. D. Porosoff, X. Yang, J. A. Boscoboinik, J. G. Chen, *Angew. Chem. Int. Ed.* **2014**, *53*, 6705-6709.
[23] M. D. Porosoff, S. Kattel, W. Li, P. Liu, J. G. Chen, *Chem. Commun.* **2015**, *51*, 6988-6991.
[24] P. Yang, H. Fu, X. Guo, B. Rachid, J. Lin, *J. Mater. Res. Technol.* **2020**, *9*, 3109-3120.
[25] A. Gupta, G. Singla, O. P. Pandey, *Ceram. Int.* **2016**, *42*, 13024-13034.
[26] C. Kunkel, F. Viñes, F. Illas, *Energy Environ. Sci.* **2016**, *9*, 141-144.
[27] J. A. Rodriguez, P. Liu, D. J. Stacchiola, S. D. Senanayake, M. G. White, J. G. Chen, *ACS Catal.* **2015**, *5*, 6696-6706.
[28] G. Kresse, J. Furthmüller, *Phys. Rev. B* **1996**, *54*, 11169-11186.
[29] G. Kresse, J. Furthmüller, *Comput. Mater. Sci.* **1996**, *6*, 15-50.
[30] J. P. Perdew, K. Burke, M. Ernzerhof, *Phys. Rev. Lett.* **1996**, *77*, 3865-3868.
[31] J. Paier, R. Hirschl, M. Marsman, G. Kresse, *J. Chem. Phys* **2005**, *122*, 234102-234114.
[32] G. Kresse, D. Joubert, *Phys. Rev. B* **1999**, *59*, 1758-1775.
[33] P. E. Blöchl, *Phys. Rev. B* **1994**, *50*, 17953-17979.
[34] S. S. Tafreshi, A. Roldan, N. H. de Leeuw, *PCCP* **2015**, *17*, 21533-21546.
[35] S. Grimme, S. Ehrlich, L. Goerigk, *J. Comput. Chem.* **2011**, *32*, 1456-1465.
[36] N. Y. Dzade, N. H. de Leeuw, *Catal.* **2021**, *11*, 127.
[37] M. Yu, D. R. Trinkle, *J. Chem. Phys.* **2011**, *134*, 064111.
[38] C. He, J. H. Zhang, W. X. Zhang, T. T. Li, *J. Phys. Chem. Lett.* **2019**, *10*, 3122-3128.
[39] L. M. Azofra, C. Sun, *R. Soc. Chem.* **2018**, DOI: 10.1039/9781782623809-00136, 136-159.
[40] Z. Ou, C. Qin, J. Niu, L. Zhang, J. Ran, *Int. J. Hydrogen Energy* **2019**, *44*, 819-834.
[41] M. G. Quesne, A. Roldan, N. H. de Leeuw, C. R. A. Catlow, *PCCP* **2019**, *21*, 10750-10760.
[42] M. G. Quesne, C. R. A. Catlow, N. H. de Leeuw, *Faraday Discuss.* **2021**, *230*, 87-99.
[43] R. A. Angnes, mechaSVG, *GitHub repository* **2020**, DOI: 10.5281/zenodo.4065333.